ELSEVIER

Earth and Planetary Science Letters 180 (2000) 243–257

EPSL

www.elsevier.com/locate/epsl

Paleomagnetic constraints on the Plio–Pleistocene geodynamic evolution of the external central–northern Apennines (Italy)

Leonardo Sagnotti *, Aldo Winkler, Laura Alfonsi, Fabio Florindo, Fabrizio Marra

Istituto Nazionale di Geofisica, Via di Vigna Murata 605, 00143 Rome, Italy

Received 20 February 2000; received in revised form 25 May 2000; accepted 29 May 2000

Abstract

We report on new paleomagnetic results obtained from 27 sites sampled in the Plio–Pleistocene sequences at the external front of the central–northern Apennines. Previous analyses of Miocene (Messinian) sediments indicated that the present shape of the northern Apenninic arc is due to the oroclinal bending of an originally straight belt oriented around N320° and that vertical axis rotations accompanied the migration of the thrust fronts toward the Adriatic foreland [F. Speranza et al., J. Geophys. Res. 102 (1997) 3153–3166]. We tried to provide new paleomagnetic constraints for the timing and rates of the oroclinal bending process during the Pliocene and the Pleistocene. The results suggest that CCW rotations observed in the northern part of the studied area are possibly younger than 3 Ma. No regional rotation is recorded in the Pliocene and Pleistocene sediments from the southern part of the study area, analogously to the Messinian sediments of the 'Acquasanta' domain of Speranza et al. [F. Speranza et al., J. Geophys. Res. 102 (1997) 3153–3166]. A local significant CCW rotation (23° ± 10°) is identified in the Early Pleistocene sediments that crop out along the Adriatic coast between Ascoli and Pescara, indicating differential motion of the thrust sheets. This rotation must be younger than 1.43 Ma.

Keywords: paleomagnetism; Apennines; tectonics; Pliocene; Pleistocene

1. Introduction

The paleomagnetic data collected in different geological environments of the Italian peninsula indicate that vertical axis rotations played a key role in the Neogene and Quaternary geodynamic evolution of the region (i.e. [2–7]). Differential rotations were recognized in structures with present-day different orientation and along curved segments of the Apenninic chain and the Calabrian Arc (see [8] for a review). A previous study of the Adriatic margin of the central–northern Apennines, in particular, pointed out that the present curvature of the Umbria–Marche–Romagna Arc is the result of an oroclinal bending of a pre-Pliocene straight belt trending roughly N320° [1]. In this case, it was suggested that rotations occurred as a result of thrust emplacement and progressive (eastward) migration of the belt. However, the actual timing of the rotational events remained unsolved because of the lack of data from Plio–

* Corresponding author. Tel.: +39-6-518601; Fax: +39-6-5041181; E-mail: sagnotti@marte.ingrm.it

0012-821X/00/$ – see front matter
PII: S0012-821X(00)00172-2

Pleistocene sediments in the area: it was only recognized that the bending episode may virtually have been produced at any time from Early Pliocene up to present [1]. Recent studies from the central and eastern Mediterranean also strongly suggest that the Neogene and Quaternary rotational episodes may occur as pulses, with surprisingly fast rates in short geological time intervals [9]; this further stresses the need of a detailed investigation of the age dependence of the rotations in each individual structure. In the present study, we report new paleomagnetic data obtained from the Plio–Pleistocene sequences cropping out at the external margin of the central–northern Apennines and discuss their bearing on the geodynamic evolution of the area.

2. Geological setting

The studied area is at the external front of the central–northern Apennines, along a coastal belt between Pescara and Pesaro (Fig. 1), where marine sediments of Plio–Pleistocene age mostly crop out. During the Plio–Pleistocene, active thrusting at the front of the central–northern Apennines caused a complex fragmentation of the former Messinian foredeep [10,11] and oroclinal bending produced the present curvature of the northern Apennines [1]. According to Calamita et al. [12], active compression migrated toward the east in five steps during the Plio–Pleistocene, reaching the structures along the present-day coast during the uppermost Early Pliocene, where it lasted up to the Pliocene–Pleistocene boundary. A recent integrated geophysical study [13] indicated that the stress field in the region had a complex evolution during the Plio–Pleistocene and two distinct areas can be recognized, with a transitional zone around 43°N. This zone is at the junction of the two arcs constituted by the northern and southern Apennines [11], that presently shows a quite different stress field: active NE–SW compression at the external (Adriatic) front of the northern Apennines [14] and active NE–SW extension in the southern Apennines [15].

As a consequence of synsedimentary tectonics, sedimentation in the area was diachronic and the

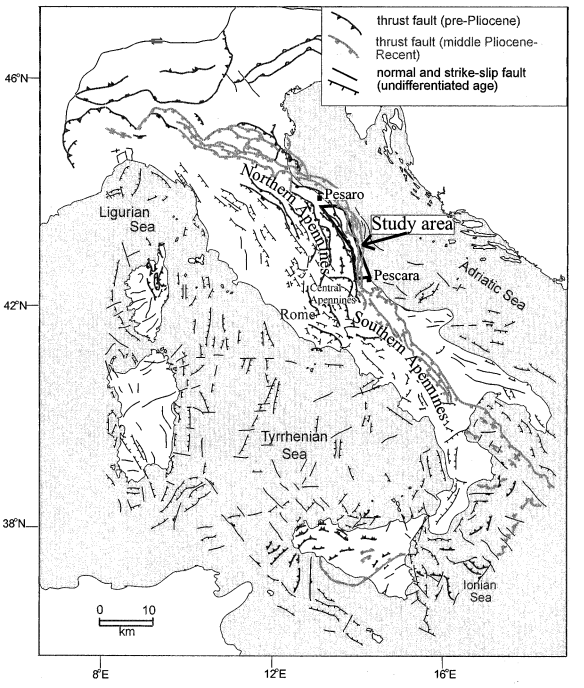

Fig. 1. Tectonic sketch of Italy (simplified from [35]) and location of the study area.

presence of hiatuses, and sometimes disconformities, identifies distinct Plio–Pleistocene depositional sequences distributed in three geographic sectors, from north to south (Fig. 2) [16,17]. In the northern and central sectors, the Lower Pliocene is represented by clays and subordinate sands, deposited in a bathyal environment (water depth ≥ 500 m). The overlying Middle Pliocene sediments are characterized by prevailing silt-clays at the base, passing to prevailing sands at the top. They show, however, a marked lateral variability that suggests an irregular topography of the depositional basin. The Pleistocene sequences are more developed in the central sector and show complex facies variation that indicates a progressive general shallowing of the basin.

In the southern sector, the Early Pliocene is represented by the Cellino Formation, with deep water turbidites that are in stratigraphic and environmental continuity with the Messinian flysch of the Laga Formation. The overlying middle and Late Pliocene sediments are composed of a thick

pelitic sequence, with coarse-grained horizons, that was deposited in a progressively deepening basin (littoral to bathyal). The Early Pleistocene sediments are also mostly pelitic and represent a regressive cycle.

3. Sampling and measurements

The samples studied in this work are the same used for the analyses of the anisotropy of magnetic susceptibility in Sagnotti et al. [13]. Standard paleomagnetic cores (25 mm diameter) were drilled and oriented in situ in 27 sites (outcrops) of fine-grained Plio–Pleistocene sediments (Fig. 2). The age distribution of the sampling sites spans the Late Early Pliocene–Middle Early Pleistocene time interval (Fig. 2).

Magnetic remanence measurements and demagnetizations were performed on a 2G cryogenic system with DC SQUID sensors in the magnetically shielded room of the Istituto Nazionale di Geofisica paleomagnetic laboratory (Rome).

For each site, two specimens from the same

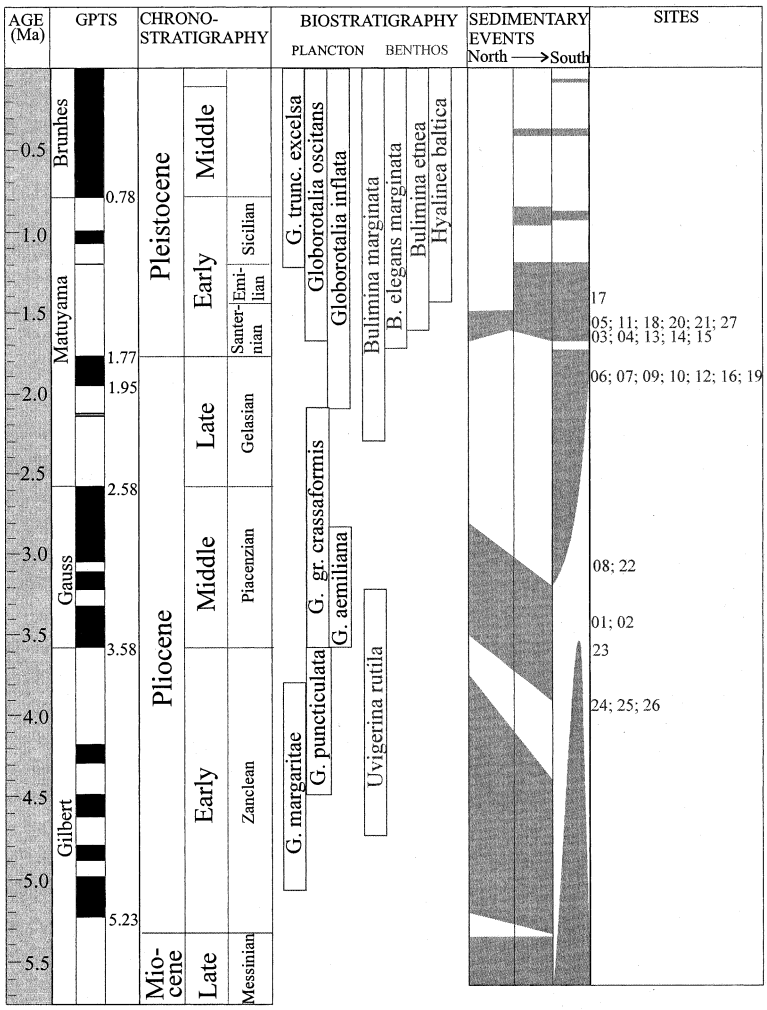

Fig. 2. Stratigraphic scheme for the study sequences (modified after [17,32]) and age of the sampling sites. The shaded areas in the 'Sedimentary events' column indicate the time represented by the sedimentary sequences along an ideal north–south transect. Geomagnetic polarity time scale is from [36].

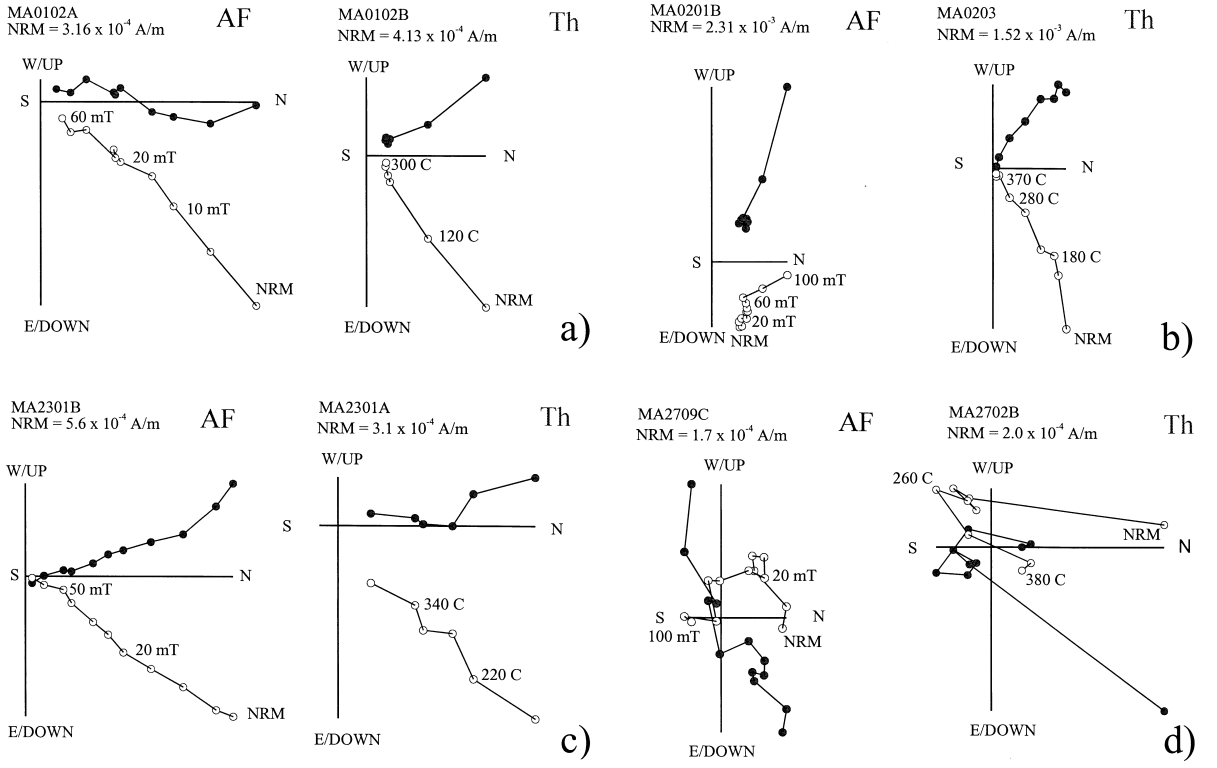

Fig. 3. Representative results from the pilot study. Orthogonal vector diagrams; tilt-corrected coordinates. Open circles, vertical projection; full circles, horizontal projection. (a) AF demagnetization more efficient than the thermal demagnetization; (b) thermal demagnetization more efficient than AF demagnetization, a significant GRM is acquired in fields >60 mT; (c) both demagnetization treatments gave reliable and consistent results; (d) neither of the two demagnetization treatments allowed the identification of a ChRM. See text for discussion.

core were selected for a pilot study: one was subjected to stepwise thermal demagnetization (steps 20, 120, 180, 220, 260, 300, 340, 380, 420°C), the other to stepwise AF demagnetization (steps 0, 5, 10, 15, 20, 25, 30, 40, 50, 60, 80, 100 mT). AF demagnetization was achieved on the 2G system, with three orthogonal demagnetization coils in line with the cryogenic magnetometer. Thermal demagnetization was carried out with a magnetically shielded electrical oven, equipped with three thermocouples for monitoring the temperatures in the heating chamber. After each thermal demagnetization step, the magnetic susceptibility was measured to monitor for alteration during heating.

The specimens selected for the pilot AF demagnetization were then subjected to stepwise demagnetization of a composite IRM [18], to identify the main magnetic carriers. We applied sequentially 2 T on the z-axis, 0.6 T on the y-axis and 0.12 T on the x-axis of the samples; thermal demagnetization of such composite IRM was carried out at 20, 120, 180, 220, 260, 300, 340, 390, 440, 490, 540, 590°C. The normalized percentage of the IRM intensity along the three axes (X%, Y% and Z%) and the maximum unblocking temperatures (T_{ub}) during the demagnetization treatment were used to evaluate the presence and the relative abundance of different magnetic minerals. For these samples, it was also measured the difference in the low-field magnetic susceptibility value along a given axis, induced by the application of a large (2 T) magnetic field at right angle (k_{diff} as defined by [19]).

Moreover, one sample for each site was selected for measurements of the hysteresis properties, us-

ing a Molspin VSM magnetometer, and of the susceptibility changes in a heating–cooling cycle from room temperature up to 700°C, using an AGICO CS-2 apparatus coupled with a KLY-2 kappabridge (see also [13]).

The results of the pilot and magnetic mineralogy studies indicated, for each site, the suitable demagnetization treatment for all the remaining samples. Seven–11 samples were stepwise demagnetized for each site. For each sample, best-fit lines or planes to progressive demagnetization data were evaluated by principal component analysis [20]. Reliability of each best-fit line and plane was estimated by the maximum angular deviation (MAD) parameter. Data with MAD $>10°$ were considered as poorly defined. Paleomagnetic site mean directions were computed using Fisher statistics [21], when only best-fit lines were computed, or the combined statistics of best-fit lines and planes [22], when remagnetization circles were also recognized.

4. Results

4.1. Pilot study and rock magnetism

Different behaviors were observed from the pilot study. For eight sites (MA01, MA03, MA04, MA07, MA10, MA18, MA19, MA20), AF demagnetization was more efficient for the isolation of a characteristic remanent magnetization (ChRM), whereas the thermal treatment produced only the removal of a low-temperature (<250°C)

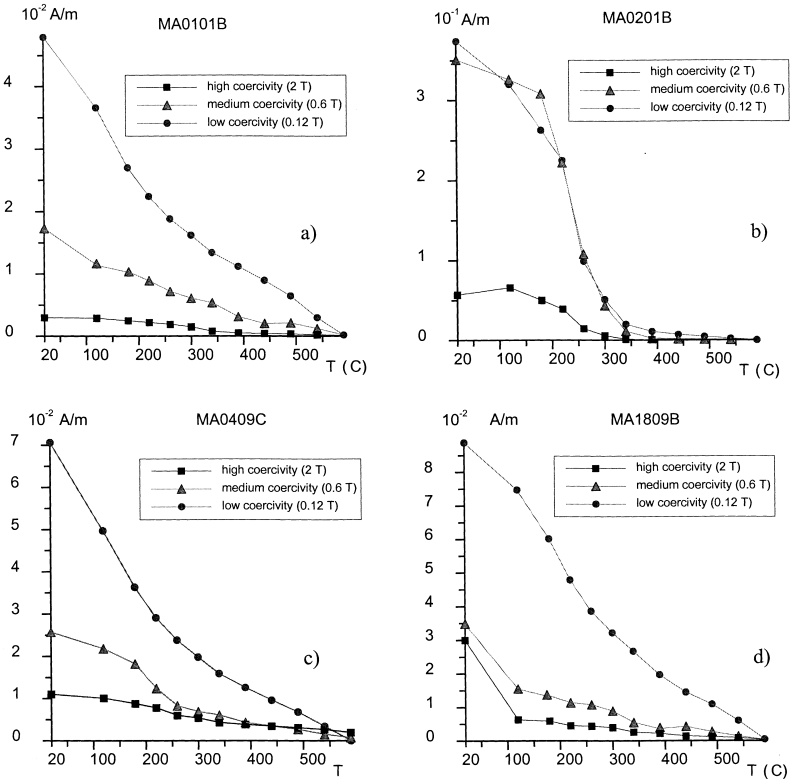

Fig. 4. Representative results of the thermal demagnetization of a composite isothermal remanence. (a) Sample with prevailing magnetite (low-coercivity and maximum unblocking temperature of ca. 590°C); (b) sample with prevailing greigite (low- to intermediate-coercivity and maximum unblocking temperature of ca. 340°C); (c) sample with a complex mixture of magnetic minerals (magnetite+greigite+hematite, the latter is suggested by a maximum unblocking temperature larger than 600°C on the high-coercivity component); (d) sample with a mixture of magnetite and goethite (intermediate- and high-coercivity with maximum unblocking temperature <120°C).

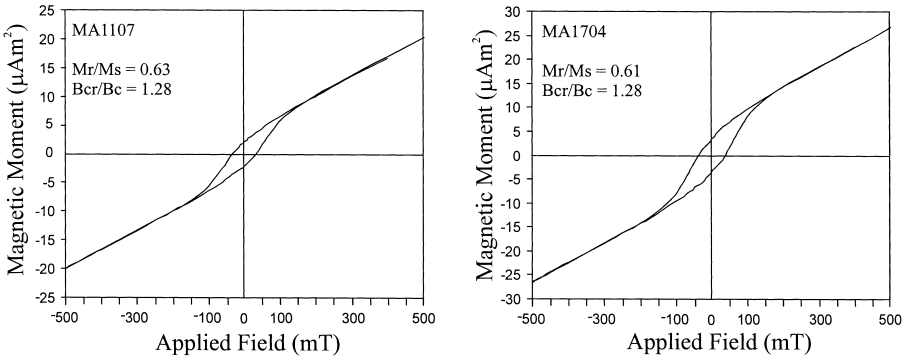

Fig. 5. Representative hysteresis loop for samples MA1107 and MA1704. The hysteresis ratios Mr/Ms (Mr = saturation remanence; Ms = saturation magnetization) and Bcr/Bc (Bcr = coercivity of remanence; Bc = coercivity) are typical of single-domain grains.

Table 1
Rock magnetic properties

Sample	k_{ini} (μSI)	k_{2T} (μSI)	k_{diff} (μSI)	T_{ub} X (°C)	T_{ub} Y (°C)	T_{ub} Z (°C)	X%	Y%	Z%	SIRM (A/m)	SIRM/k (kA/m)
MA0101B	107	107	0	590	(390); 590	(340–390)	88.2	11.5	0.3	0.051	0.5
MA0201B	158	160	2	340	340; (590)	340	52.5	46.3	1.2	0.516	3.3
MA0306B	89	89	0	590	340; 590	–	93.4	6.1	0.5	0.080	0.9
MA0409C	115	115	0	590	260; 590	> 590	86.4	11.5	2.1	0.076	0.7
MA0501B	239	260	21	260; 390	260	260	96.7	3.1	0.2	6.254	26.2
MA0602	101	101	0	590	590	–	92.3	7.0	0.7	0.091	0.9
MA0705A	100	101	1	590	260; 590	–	88.1	9.7	2.2	0.089	0.9
MA0801	101	101	0	590	(590)	–	94.2	5.2	0.5	0.070	0.7
MA0903	75	75	0	590	590	–	85.8	13.0	1.2	0.047	0.6
MA1003A	145	146	1	260; 390; 590	260; 390	(260)	78.7	20.1	1.2	0.574	4.0
MA1103B	262	291	29	260; 340	340	340	77.9	18.8	3.3	10.196	38.9
MA1204C	241	269	28	340	340	340	82.1	17.4	0.5	14.494	60.1
MA1303C	154	156	2	390;(590)	390	340	80.3	19.3	0.4	1.169	7.6
MA1402B	180	186	6	(260); 390	390	340	81.8	16.6	1.6	3.705	20.6
MA1507B	215	231	16	390; (590)	390	390	63.9	34.8	1.3	0.863	4.0
MA1609A	188	191	3	340	340	340	72.5	26.5	1.0	2.255	12.0
MA1710B	215	231	16	390	390	390	72.1	25.9	2.1	7.433	34.6
MA1809B	119	119	0	590	120; (390); 590	120	78.8	12.2	9.0	0.100	0.8
MA1909A	183	184	1	390; 590	390	390	64.0	34.9	1.1	0.672	3.7
MA2008B	101	101	0	590	340; 590	–	83.3	15.7	1.0	0.084	0.8
MA2108B	181	191	10	340–390	340–390	340–390	77.0	22.4	0.6	5.095	28.1
MA22test	135	135	0	590	(340)	–	95.8	4.1	0.1	0.114	0.8
MA2306B	150	150	0	590	(340)	(340)	85.3	13.6	1.0	0.136	0.9
MA2409	164	164	0	590	590	–	89.0	7.4	3.6	0.139	0.9
MA2510A	317	363	46	340	260	340	98.5	0.3	1.2	15.316	48.3
MA2602A	215	225	10	390	390	390	73.4	24.7	1.9	6.735	31.3
MA2703A	147	148	1	(340); 590	340; (590)	(340)	88.1	11.0	0.9	0.160	1.1

k_{ini} = initial susceptibility; k_{2T} = susceptibility after application of a 2 T field at right angle from the direction of measurement; $k_{diff} = k_{2T} - k_{ini}$. T_{ub} (X, Y and Z), main inflection points for the X, Y and Z curves during stepwise demagnetization of a composite remanence (see text). X, Y and Z (%): percentage of the composite IRM on the respective axis at 20°C. SIRM: total IRM at 2 T.

Table 2
Paleomagnetic results

Site	Method	Max stab.	N (c, l)	Decl atc	Incl atc	k	α_{95}	Decl btc	Incl btc	Biostratigraphic zonation
Early–Middle Pliocene										
MA01	AF	100 mT	8 (2, 6)	347.6	57	37.6	9.3	1.1	65.2	U. rutila
MA02	Th	370°C	10 (0, 10)	332.7	45	64.8	6.0	351.5	53.3	U. rutila
MA08[a]	Th	250°C	8 (7, 1)	327.5	54.6	27.6	11	1.4	49.6	G. aemiliana
MA22[a]	Th	250°C	9 (0, 9)	52.5	49.4	20.2	11.7	44.6	68.9	G. aemiliana
MA23	AF	60 mT	9 (0, 9)	1	45.2	93.2	5.4	341.4	55.8	barren, Cellino Fm
MA24	Th	370°C	9 (3, 6)	153.5	−75.7	41.4	8.3	96.8	−51.1	scarce fauna, Cellino Fm
MA25	Th	370°C	10 (0, 10)	203.1	−33.9	369.5	2.5	148.6	−54.5	barren, Cellino Fm
MA26	Th	420°C	8 (0, 8)	166.6	−68.8	42.6	8.6	222.1	−67.8	G. puncticulata/margaritae
Late Pliocene										
MA06[a]	Th	250°C	8 (0, 8)	20.1	40.4	33.7	9.7	18.9	22.5	B. marginata
MA07	AF	100 mT	12 (0, 12)	–	–	48.6	6.3	357.4	47.7	B. marginata
MA09[a]	Th	220°C	10 (0, 10)	11.8	43	29.7	9	6.5	54.1	B. marginata
MA10	AF	90 mT	8 (3, 5)	355.8	63.6	33.6	10	345.1	56.9	B. marginata
MA12	Th	370°C	11 (0, 11)	359.2	47	39.5	7.4	354.5	52.8	G. inflata
MA16	Th	370°C	7 (2, 5)	–	–	94.5	6.4	340.7	54.4	B. marginata
MA19	AF	100 mT	11 (0, 11)	330.8	47.6	48.2	6.6	325.2	51.2	B. marginata
Early Pleistocene										
MA03	AF	100 mT	8 (0, 8)	–	–	72.1	6.6	356.1	60	B. marg., B. elegans marg.
MA04[a]	AF	60 mT	9 (0, 9)	298.9	62.5	9.9	17.2	288.4	57.3	B. marg., B. elegans marg.
MA05[a]	Th	460°C	9 (3, 6)	147.1	−64	492.1	2.4	122.2	−45.3	B. etnea
MA11[a]	Th	370°C	8 (0, 8)	51.3	−33.6	27	10.9	52.4	−27.9	B. eleg. marg., B. cfr. etnea
MA13[a]	Th	310°C	8 (0, 8)	338.9	43	21.6^{atc} 117.6^{btc}	12.2^{atc} 5.1^{btc}	353.8	56.2	B. marg., B. elegans marg.
MA14	Th	460°C	8 (0, 8)	–	–	57.5	7.4	183.1	−63.8	B. marg., B. elegans marg.
MA15	Th	460°C	11 (6, 5)	–	–	41.2	7.4	143.8	−49.6	G. oscitans
MA17	Th	400°C	10 (0, 10)	–	–	60.1	6.3	159.5	−48.8	H. baltica
MA18	AF	100 mT	10 (0, 10)	–	–	61.8	6.2	344.7	55.5	B. etnea
MA20	AF	100 mT	8 (0, 8)	–	–	34.6	9.6	346.9	60.2	B. cfr. etnea
MA21	Th	370°C	9 (0, 9)	191.4	−64.2	798.8	1.8	168.5	−64	B. cfr. etnea
MA27[a]	Th	370°C	7 (0, 7)	322.6	−78.3	3.8	36	210.2	−84.1	B. etnea

Max stab.: maximum magnetic field or temperature (for AF or thermal demagnetization, respectively) used in the principal component analysis of the demagnetization data; N: number of samples (c = number of remagnetization circles; l = number of stable directions); Decl = declination of the ChRM; Incl = inclination of the ChRM; atc = after tectonic correction; btc = before tectonic correction; k and α_{95}, statistical parameters after [21].
[a]Discarded sites (see text for explanation).

component and no significant demagnetization at higher temperatures (Fig. 3a) or noisy demagnetization diagrams; for such sites, the main magnetic carrier was identified as magnetite (Fig. 4a). For other 11 sites (MA02, MA05, MA11, MA13, MA14, MA16, MA17, MA21, MA24, MA25, MA26), thermal demagnetization gave better results, whereas AF treatment did not significantly demagnetize the samples and/or resulted in the acquisition of gyro-remanences for fields higher than 40–50 mT (Fig. 3b); in such sites, the main magnetic mineral is a magnetic iron sulphide, most likely greigite (Fig. 4b). For three sites (MA12, MA15, MA23), both demagnetization treatments gave good, and consistent, results (Fig. 3c). Two of these sites (MA12 and MA15) showed iron sulphides as the main magnetic minerals and were demagnetized thermally; the third site (MA23) showed prevailing magnetite and was demagnetized AF. Finally, for five sites (MA06, MA08, MA09, MA22, MA27), with magnetite as the main magnetic carrier, neither of the two treatments allowed the clear identification of a ChRM or provided interpretable demagnetization

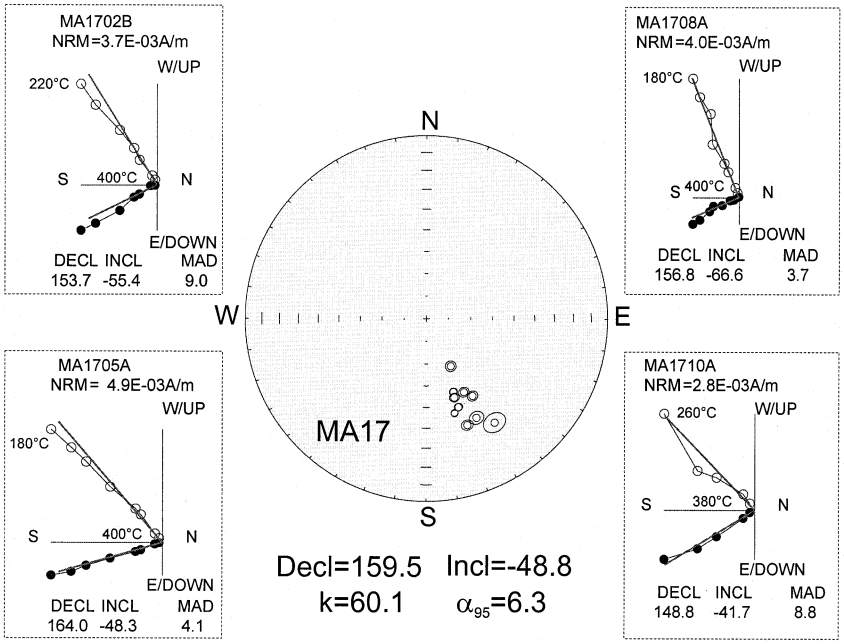

Fig. 6. Paleomagnetic data for site MA17. Equal area projection and orthogonal vector diagrams; tilt-corrected coordinates. Linear best fits to the demagnetization data are also reported. Demagnetization data allow the identification of a stable ChRM and the paleomagnetic site mean direction is well defined.

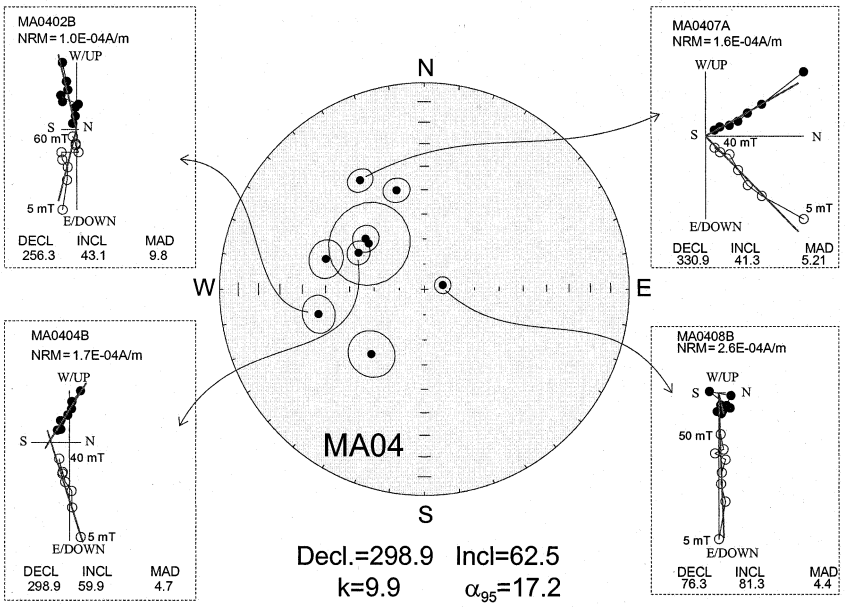

Fig. 7. Paleomagnetic data for site MA04. Equal area projection and orthogonal vector diagrams; tilt-corrected coordinates. Linear best fits to the demagnetization data are also reported. Even though the demagnetization data allow the identification of a stable ChRM in most of the samples, the paleomagnetic data are largely scattered at the site level and the mean direction is aberrant.

paths (Fig. 3d); nevertheless, these sites were tentatively demagnetized thermally. The presence of high-coercivity minerals was identified only at site MA04, with a complex magnetic mixture of magnetite, iron sulphides and hematite (Fig. 4c), and at site MA18, that shows the presence of goethite and magnetite (Fig. 4d). Hysteresis cycles and k versus temperature curves indicate that the paramagnetic contribution of the clay matrix overwhelms the ferromagnetic contribution at 21 out of the 27 sites (see [13]), however, hysteresis cycles of samples with prevailing iron sulphides show characteristics typical of single-domain grains (Fig. 5). Samples with magnetic iron sulphides show also a typical field impressed anisotropy, with a k_{diff} distinctly larger than zero, and a relatively high SIRM/k value (Table 1), both properties also indicating a single-domain state. Samples with magnetite as the main magnetic carrier always show $k_{diff} = 0$ (Table 1). This provides a further experimental verification of the suitability of the k_{diff} parameter to distinguish between greigite-bearing and magnetite-bearing sediments [19].

4.2. Paleomagnetism

Analysis of demagnetization data allowed the determination of linear paths or remagnetization circles for most of the samples. Paleomagnetic site mean directions are listed in Table 2. Well defined (i.e. $\alpha_{95} < 10°$) and stable paleomagnetic directions were found for 19 sites (Fig. 6), three sites (MA04, MA11, MA27) showed a wide scattering (i.e. $\alpha_{95} > 10°$) of paleomagnetic data (Fig. 7) or well defined but aberrant paleomagnetic directions (Fig. 8). Finally, four sites (MA06, MA08, MA09, MA22) showed only a low-temperature component (unblocked at temperatures $< 250°C$), that is interpreted as of viscous origin. Tilting of the sediments is limited ($< 10°$) for the Late Pliocene–Early Pleistocene sequences and bedding is almost sub-horizontal in most of such sites (one exception, site MA05, is discussed be-

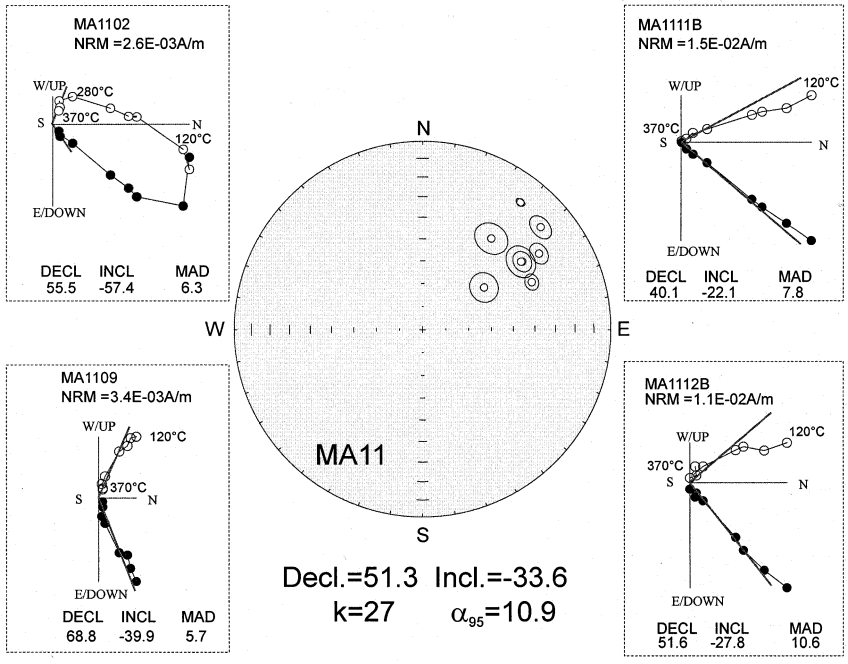

Fig. 8. Paleomagnetic data for site MA11. Equal area projection and orthogonal vector diagrams; tilt-corrected coordinates. Linear best fits to the demagnetization data are also reported. Demagnetization data allow the identification of a stable ChRM and paleomagnetic data are grouped at the site level, but the site mean direction is aberrant.

low), so that no tectonic correction was applied in eight sites. However, tilting of the strata is significant for the older (Early Pliocene) sites and reaches 53° at site MA25 in the Cellino Formation. Site MA05 is dated as Emilian in age and shows a tilting of the beds of about 25°: it was discarded for tectonic reconstruction since it is considered not in place (see [13]). At only one site (MA13), bedding had different attitudes within the sampled outcrop; at this site, paleomagnetic data are more clustered before than after tectonic correction and the main magnetic carrier is greigite (Table 1), indicating remagnetization due to a late (post-tilting) authigenic growth of iron sulphides.

Sites distribution, paleomagnetic mean declinations and uncertainties (computed as $\sin^{-1}(\sin \alpha_{95}/\cos I)$) are shown in the geological map of Fig. 9, together with the paleomagnetic results previously obtained from the Messinian sediments [1,23,24].

5. Discussion

Following the above results and analysis, only 18 sites provided paleomagnetic data that may be reliable for tectonic purposes (see Table 2 and Fig. 9). In particular, they are six sites of Early–Middle Pliocene age and 12 sites of Late Plio-

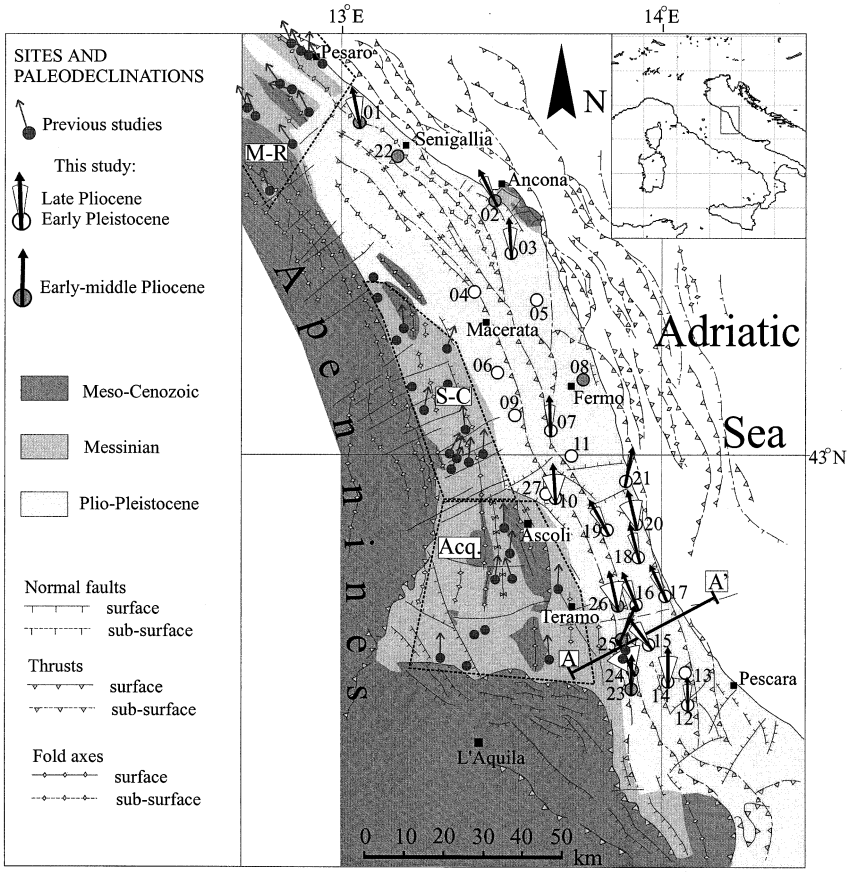

Fig. 9. Geological sketch of the study area (redrawn from [29,30]) and main paleomagnetic results. Data and sites from previous studies are from [1,23,24]. Uncertainties on the paleomagnetic declinations were computed as $\sin^{-1}(\sin \alpha_{95}/\cos I)$. A–A′ line indicates the trace of the geologic profile shown in Fig. 12. Areas boxed with dashed lines in the Messinian sediments indicate the structural–paleomagnetic domain distinguished by Speranza et al. [1]: M–R: 'Marche–Romagna domain'; S–C: 'Sibillini–Cingoli domain'; Acq.: 'Acquasanta domain'. See text for explanations.

cene–Early Pleistocene age. Paleomagnetic directions were compared to the present-day geocentric axial dipole (GAD) field: in order to estimate vertical axis rotations, the obtained paleomagnetic declinations were compared to the local meridian. Caution was used in the tectonic interpretation of paleomagnetic site mean directions close to the present-day GAD field in in situ coordinates and with a low-temperature stability of the ChRM (sites MA01, MA03, MA07, MA10, MA18 and MA20), that may indicate recent remagnetization.

GAD inclinations in the sampled region are expected to be around 61.8°. The observed paleomagnetic inclinations are comprised between 33° and 76° (after tectonic correction; see Fig. 10) and the inclination flattening is generally less developed than in the older sediments of the Apennines [1]. Nevertheless, paleomagnetic inclination is significantly shallower than the expected GAD value for most of the sites. Such inclination flattening can be linked to the effect of compaction in fine-grained sediments [25,26]. Paleomagnetic declinations indicate that there are both rotated and not-rotated sites. Early–Middle Pliocene sediments show that two sites in the northern part of the study area (MA01 and MA02) indicate CCW rotations that are similar to those reported for the contiguous Messinian sites (Fig. 9 and Table 2). However, the two sites are both of normal polarity and the paleomagnetic directions are not rotated in geographic coordinates (Table 2), so that the possibility of a recent remagnetization cannot be ruled out. The Early–Middle Pliocene sediments from the southern region (sites MA23–MA26) show a large dispersion in both declinations and inclinations (Figs. 9 and 10), but on average they do not indicate significant regional rotations, in agreement with the results from the internal (western) Messinian sites [1,23] and from the eastern Late Pliocene to Early Pleistocene sites (MA12 and MA14). The Late Pliocene and Early Pleistocene sites north of Ascoli do not allow firm conclusions: they indicate either a possible null rotation (sites MA10, MA07 and MA03; but they may have been remagnetized, following the principles discussed above) or a slight clockwise rotation (site MA21) similar to that observed in

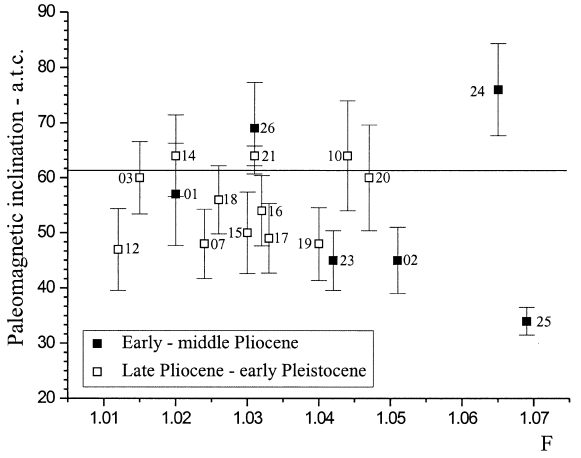

Fig. 10. Plot of magnetic foliation ($F = k_{int}/k_{min}$) data (from [13]) versus paleomagnetic inclination after tectonic correction (a.t.c.). Numbers close to each symbol indicate the site number.

the internal Messinian sites of the 'Sibillini–Cingoli' domain [1]. On the other hand, a small area is identified in which six sites (MA15–MA20) provided consistent evidences for a significant CCW rotation (Fig. 9). The combined analysis of the paleomagnetic results from these six sites, in tilt-corrected coordinates reported all to normal polarity, gives: declination = 337.1°, inclination = 53.0°, $\alpha_{95} = 6.0°$, indicating a CCW rotation of 23° ± 10° (Fig. 11). The age of these six sites is in the range Late Pliocene (sites MA16 and MA19)–Early Pleistocene (sites MA15, MA17, MA18 and MA20) (Fig. 2 and Table 2). Magnetic polarity of sites MA16 and MA19 (normal) and of sites MA15 and MA17 (reverse) is consistent with their biostratigraphic age (Fig. 2). However, normal polarity of sites MA18 and MA20 is not consistent with their biostratigraphic age. Such two sites may have been remagnetized during the Brunhes Chron (age < 0.78 Ma). Site MA18 shows also evidence for goethite and this reinforces the hypothesis of a possible remagnetization. Such two sites are sub-horizontal and no tectonic correction was applied to their paleomagnetic data. The in situ paleomagnetic data are rotated CCW (ca. 15°) from the direction of the present-day GAD field, even if the GAD direction is in the 95% confidence region of site MA20 (see Ta-

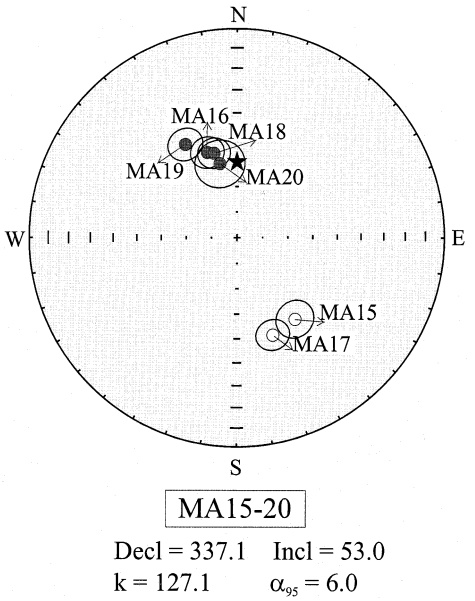

Fig. 11. Equal area projection of paleomagnetic data for sites MA15–MA20. Tilt-corrected coordinates. Full circles: normal polarity (lower hemisphere); open circles: reverse polarity (upper hemisphere). Ellipses around the mean direction indicate the cone of 95% of confidence. The black star indicates the direction of the GAD field in the study area.

ble 2 and Fig. 11). These data imply that at least part of the CCW rotation is younger than 0.78 Ma. Similar fast and young tectonic rotations are being increasingly reported from different regions of the Mediterranean area [4,27,28].

Neogene vertical axis rotation in the northern and central Apennines is referred to thrust emplacement [1] or to strike-slip faults and out of sequence thrust activity [6]. The area affected by the rotation identified in this study is structurally and geographically limited (Fig. 9). Anyway, the identification of the structures along which the rotation occurred is not straightforward, since no major structural element crops out in the discussed area. The main structures are buried fronts of thrust sheets that do not reach the surface (see Figs. 9 and 12) [29–31]. All the rotated sites are, in particular, located between two buried thrust fronts, that in the regional geological literature are known as 'Cellino structure' (western; between sites 25–26 and 15–16 in Fig. 9) and 'Campomare' [16] or 'Costiera' [32] structure (eastern; just east of sites 20 and 17 in Fig. 9). The 'Cellino' structure in the western margin of the rotated area trends N340° to N–S; the 'Costiera' structure, to the eastern margin of the rotated area, trends about N340° (see [30]). Just westward of the rotated area, in a more internal position of the Apenninic chain, the geological structures are oriented N–S and the paleomagnetic sites indicate no rotation (see also [1,23]). The difference in the trend of the thrust fronts along a west–east transect running at the latitude of Teramo is compatible with the paleomagnetic data. This would imply that the thrusts of the 'Costiera' structure are decoupled from the more internal ones and

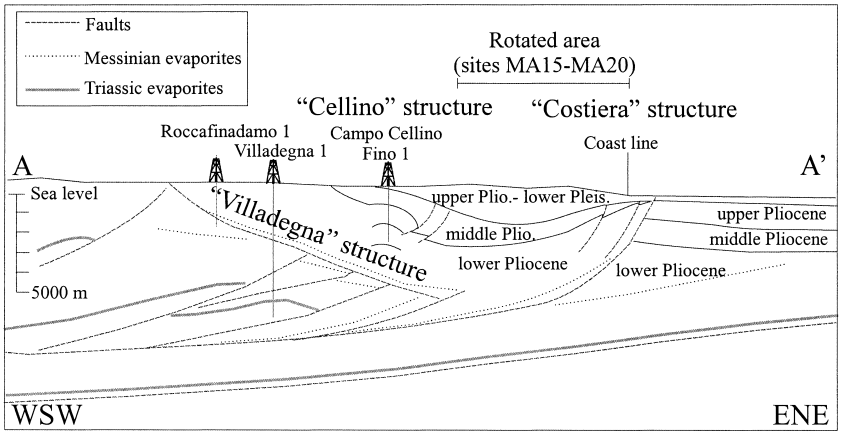

Fig. 12. Schematic geologic profile across the 'Villadegna', 'Cellino' and 'Costiera' structures, from analysis of seismic reflection profiles and wells (redrawn after [33,34]). The trace of the profile is indicated as A–A′ in Fig. 9. See text for discussion.

that they differentially advanced toward the east carrying passively on top the undeformed Plio–Pleistocene sedimentary sequences (Fig. 12). As a matter of fact, the 'Costiera' structure is detached at the level of the Messinian evaporites, whereas the western (internal) structures are mostly detached at the level of the Triassic evaporites [32,33]. It is also remarkable that along the western margin of the rotated area traces of surficial NE-dipping normal faults are reported [29] and subsurficial east-dipping faults are also known from the analysis of seismic reflection profiles and wells [33], associated to the eastward verging 'Villadegna' structure (Fig. 12). These faults may account for the extension induced by the differential eastward propagation and uplift of the 'Costiera' structure. The Plio–Pleistocene sequences between these two structures are arranged in a broad synclinorium; the synsedimentary tectonic activity and uplift of the 'Costiera' structure induced the backward (westward) shifting of the depocenter of the Pliocene basin [32,34] (Fig. 12). The eastward verging 'Villadegna' structure fades out toward the north, and north of Ascoli (i.e. north of the CCW rotated block) it is no more visible in seismic profiles [33]. A possible further tectonic element that may account for the observed rotation is inferred from a characteristic bend in the more external thrusts, in the Adriatic Sea to the east of the rotated area, that show a strike rotation from N340° to N15° (Fig. 9). The ideal southward prosecution of such tectonic structures separates rotated (MA15 and MA17) and not rotated sites (MA12 and MA14) and could constitute the southern boundary of the rotated area, suggesting that such external thrusts pass and merge into a transfer fault oriented NNE–SSW, with a dextral strike-slip kinematics.

6. Conclusions

The paleomagnetic data from the Plio–Pleistocene sequences at the external front of the central–northern Apennines provide new constraints for the reconstruction of the vertical axis rotations that accompanied the migration of the thrust fronts toward the Adriatic foreland and induced the present-day curvature of the belt. In particular, the new paleomagnetic data indicate that:

- The post-Messinian CCW rotations ($\sim 20°$) of northern sector ('Marche–Romagna domain' [1], see Fig. 9) are possibly younger than 3 Ma (Middle Pliocene – U. rutila zone), but data from the new sites are not rotated in geographic coordinates and remagnetization cannot be ruled out
- Between Ascoli and Ancona (east of the 'Sibillini–Cingoli' domain [1]), paleomagnetic results suggest no paleomagnetic rotation or weak clockwise rotations
- No rotation is also recorded by the Early Pliocene sediments of the Cellino Formation east of Teramo (analogously to the Messinian sediments of the 'Acquasanta domain' [1], see Fig. 9) and by the Early Pleistocene sediments just to the west of Pescara
- A significant CCW rotation ($23° \pm 10°$) is identified in the Early Pleistocene sediments that crop out in a belt parallel to the coast between Ascoli and Pescara. This rotation must be younger than 1.43 Ma (FO of Hyalinea baltica – site MA17); and possibly younger than 0.78 Ma (if sites MA18 and/or MA20 are remagnetized). This CCW rotation affects an area comprised between two buried structures, with a local trend of NNW–SSE. Paleomagnetic data suggest a decoupling between this area and the internal 'Acquasanta' domain and a differential eastward migration of the thrusts of the 'Costiera' structure.

Acknowledgements

We thank Enzo Boschi, who encouraged this work. Reviews by Giovanni Muttoni and Cor Langereis improved the paper.*[RV]*

References

[1] F. Speranza, L. Sagnotti, M. Mattei, Tectonics of the Umbria–Marche–Romagna Arc (central northern Apen-

nines, Italy): new paleomagnetic constraints, J. Geophys. Res. 102 (1997) 3153–3166.
[2] L. Sagnotti, Paleomagnetic evidence for a Pleistocene counterclockwise rotation of the Sant'Arcangelo basin, Geophys. Res. Lett. 19 (1992) 135–138.
[3] P.J.J. Scheepers, C.G. Langereis, F.J. Hilgen, Counterclockwise rotations in the southern Apennines during the Pleistocene: paleomagnetic evidence from the Matera area, Tectonophysics 225 (1993) 379–410.
[4] P.J.J. Scheepers, C.G. Langereis, Paleomagnetic evidence for counter-clockwise rotations in the southern Apennines fold-and-thrust belt during the Late Pliocene and middle Pleistocene, Tectonophysics 239 (1994) 43–59.
[5] P.J.J. Scheepers, Tectonic rotations in the Tyrrhenian arc system during the Quaternary and late Tertiary, Geol. Ultraj. 112 (1994) 1–352.
[6] M. Mattei, R. Funiciello, C. Kissel, Paleomagnetic and structural evidence for Neogene block rotations in the Central Apennines, Italy, J. Geophys. Res. 100 (1995) 17863–17883.
[7] G. Muttoni, A. Argnani, D.V. Kent, N. Abrahamsen, U. Cibin, Paleomagnetic evidence for Neogene tectonic rotations in the northern Apennines, Earth Planet. Sci. Lett. 154 (1998) 25–40.
[8] A. Meloni, L. Alfonsi, F. Florindo, L. Sagnotti, F. Speranza, A. Winkler, Neogene and Quaternary geodynamic evolution of the Italian peninsula: the contribution of paleomagnetic data, Ann. Geofis. XL 3 (1997) 705–727.
[9] C.E. Duermeijer, Neogene to Recent tectonic evolution of the central Mediterranean: an integrated paleomagnetic approach, Ph.D. thesis, Utrecht University, Geol. Ultraj. 176, 1999, 168 pp.
[10] F. Ricci Lucchi, The Oligocene to Recent foreland basins of the northern Apennines, Spec. Publ. Int. Ass. Sediment. 8 (1986) 105–139.
[11] E. Patacca and P. Scandone, Post-Tortonian mountain building in the Apennines: the role of the passive sinking of a relic lithospheric slab, in: A. Boriani, M. Bonafede, G.B. Piccardo and G.B. Vai (Eds.), The Lithosphere in Italy Advances in Earth Science Research, Accademia Nazionale dei Lincei, Mid Term Conference, Rome, 5–6 May 1987, 1989, pp. 157–176.
[12] F. Calamita, G. Cello, G. Deiana, Structural styles, chronology rates of deformation, and time-space relationships in the Umbria–Marche thrust system (central Apennines, Italy), Tectonics 13 (1994) 873–881.
[13] L. Sagnotti, A. Winkler, P. Montone, L. DiBella, F. Florindo, M.T. Mariucci, F. Marra, L. Alfonsi, A. Frepoli, Magnetic anisotropy of Plio–Pleistocene sediments from the Adriatic margin of the northern Apennines (Italy): Implications for the time-space evolution of the stress-field, Tectonophysics 311 (1999) 139–153.
[14] M.T. Mariucci, A. Amato, P. Montone, Recent tectonic evolution and present stress in the northern Apennines, Tectonics 18 (1999) 108–118.
[15] A. Amato, P. Montone, Present-day stress field and active tectonics in southern peninsular Italy, Geophys. J. Int. 130 (1997) 519–534.
[16] U. Crescenti, C. D'Amato, A. Balduzzi, M. Tonna, Il Plio–Pleistocene del sottosuolo abruzzese-marchigiano tra Ascoli Piceno e Pescara, Geol. Rom. 19 (1980) 63–84.
[17] G. Cantalamessa, E. Centamore, U. Chiocchini, M.L. Colalongo, A. Micarelli, T. Nanni, G. Pasini, M. Potetti, F. Ricci Lucchi, C. Cristallini and L. Di Lorito, Il Plio–Pleistocene delle Marche, Studi Geologici Camerti, Special Volume 'La Geologia delle Marche', 1986, pp. 61–81.
[18] W. Lowrie, Identification of ferromagnetic minerals in a rock by coercivity and unblocking temperature properties, Geophys. Res. Lett. 17 (1990) 159–162.
[19] L. Sagnotti, A. Winkler, Rock magnetism and palaeomagnetism of greigite-bearing mudstones in the Italian peninsula, Earth Planet. Sci. Lett. 165 (1999) 67–80.
[20] J.L. Kirschvink, The least-squares line and plane and the analysis of paleomagnetic data, Geophys. J. R. Astron. Soc. 62 (1980) 699–718.
[21] R.A. Fisher, Dispersion on a sphere, Proc. R. Soc. Lond. A217 (1953) 295–305.
[22] P.L. McFadden, M.W. McElhinny, The combined analysis of remagnetization circles and direct observations in paleomagnetism, Earth Planet. Sci. Lett. 87 (1988) 161–172.
[23] F. DelaPierre, F. Ghisetti, R. Lanza, L. Vezzani, Paleomagnetic and structural evidence of Neogene tectonic rotation of the Gran Sasso range (central Apennines, Italy), Tectonophysics 215 (1992) 335–348.
[24] L. Lanci and C.F. Wezel, Rotazioni tettoniche di eta' Messiniana nell'Appennino marchigiano, in: Geodinamica e Tettonica Attiva del Sistema Tirreno–Appennino (Abstracts), Univ. Studi Camerino, Camerino, 1995, pp. 330–332.
[25] P. Arason, S. Levi, Models of inclination shallowing during sediment compaction, J. Geophys. Res. 95 (B4) (1990) 4481–4499.
[26] G.A. Deamer, K.P. Kodama, Compaction-induced inclination shallowing in synthetic and natural clay-rich sediments, J. Geophys. Res. 95 (1990) 4511–4529.
[27] C.E. Duermeijer, C.G. Langereis, Astronomical dating of a tectonic rotation on Sicily and consequences for the timing and extent of the Mid-Pliocene deformation phase, Tectonophysics 298 (1998) 243–258.
[28] C.E. Duermeijer, W. Krijgsman, C.G. Langereis, J.E. Meulenkamp, M.V. Triantaphyllou, W.J. Zachariasse, A late Pleistocene clockwise rotation phase of Zakynthos (Greece) and implications for the evolution of the western Aegean arc, Earth Planet. Sci. Lett. 173 (1999) 315–331.
[29] P. Ambrosetti, C. Bosi, F. Carraro, N. Ciaranfi, M. Panizza, G. Papani, L. Vezzani and A. Zanferrari, Neotectonic Map of Italy, Scale 1:500 000, PFG-CNR, Quad. Ric. Sci. 114, Vol. 4, 1983.
[30] G. Bigi, D. Cosentino, M. Parotto, R. Sartori and P. Scandone, Structural Model of Italy, Scale 1:500 000, PFG-CNR, Quad. Ric. Sci. 114, Vol. 3., 1991.

[31] L. Vezzani and F. Ghisetti, Carta Geologica dell'Abruzzo, Scale 1:100 000, Selca, Firenze, 1998.
[32] G.G. Ori, G. Serafini, C. Visentin, F. Ricci Lucchi, R. Casnedi, M.L. Colalongo and S. Monna, The Plio–Pleistocene Adriatic foredeep (Marche and Abruzzo, Italy): an integrated approach to surface and subsurface geology, 3rd European Ass. Petroleum Geology Conference, May 1991, Adriatic Foredeep Field Trip Guide Book, 1991, pp. 1–85.
[33] A.W. Bally, L. Burbi, C. Cooper, R. Ghelardoni, Balanced sections and seismic profiles across the Central Apennines, Mem. Soc. Geol. It. 35 (1986) 257–310.
[34] R. Casnedi, L'avanfossa abruzzese tra i fiumi Vomano e Pescara nel Pliocene inferiore: rapporti fra sedimentazione e tettonica, Studi Geologici Camerti, Special Volume (1991/2) 'CROP 11', 1991, pp. 375–379.
[35] G. Bigi, A. Castellarin, R. Catalano, M. Coli, D. Cosentino, G.V. Dal Piaz, F. Lentini, M. Parotto, E. Patacca, A. Praturlon, F. Salvini, R. Sartori, P. Scandone and G.B. Vai, Synthetic structural-kinematic map of Italy, Scale 1:2 000 000, PFG-CNR, 1989.
[36] S.C. Cande, D.V. Kent, Revised calibration of the geomagnetic polarity timescale for the Late Cretaceous and Cenozoic, J. Geophys. Res. 100 (1995) 6093–6095.